



## The Local Surface Heat Transfer Coefficient in Thermal Food Process Calculations: A CFD Approach

Pieter Verboven,\* Bart M. Nicolai, Nico Scheerlinck  
& Josse De Baerdemaeker

Department of Agro-Engineering and -Economics, K.U. Leuven, Kardinaal Mercierlaan 92,  
B-3001 Heverlee, Belgium

(Received 16 January 1997; accepted 22 May 1997)

### ABSTRACT

*The surface heat transfer coefficient during thermal processing of foods of different shapes and for different heating conditions has been calculated using Computational Fluid Dynamics techniques and compared to experimental results obtained from the literature. The calculated product-averaged coefficients are a maximum of 14% smaller than the experimental values. For Reynolds numbers lower than 10,000, the calculated local distribution corresponds to the experimental pattern. Variations in the product temperatures are evaluated using a finite element model for heat conduction. For the cases studied, the simulations indicate that the product temperature change as a result of local variations of the surface heat transfer coefficient is slower than that obtained under the assumption of a homogeneous surface heat transfer coefficient. Further, the coldest spot is no longer at the geometric centre. © 1997 Elsevier Science Limited.*

### NOMENCLATURE

$C_f$	Specific heat capacity of the heating medium, W/kg°C
$C_p$	Specific heat capacity of the food product, W/kg°C
$D$	Height of the product, m
$f$	Shedding frequency, 1/s
$Fo$	Dimensionless Fourier number, $(\alpha_p t)/[(D/2)^2]$ ,

\*To whom all correspondence should be addressed. Tel. (+32) 16 321441; fax (+32) 16 321994; e-mail: pieter.verboven@agr.kuleuven.ac.be.

$h$	Enthalpy, J/kg
$h_x$	Local surface heat transfer coefficient, $\text{W/m}^2\text{°C}$
$\bar{h}$	Product-averaged surface heat transfer coefficient, $\text{W/m}^2\text{°C}$
$k_f$	Thermal conductivity of the heating medium, $\text{W/m}^2\text{°C}$
$k_p$	Thermal conductivity of the food product, $\text{W/m}^2\text{°C}$
$L$	Width of the product, m
$Nu_D$	Dimensionless Nusselt number, $h_x D/k_f$
$\overline{Nu}_D$	Dimensionless product-averaged Nusselt number, $\bar{h} D/k_f$
$p$	Pressure of the heating medium, Pa
$Re_D$	Dimensionless Reynolds number, $(U_\infty D)/\nu$
$S$	Dimensionless Strouhal number, $fD/U$
$\mathbf{U}$	Velocity vector of the heating medium, m/s
$U_\infty$	Magnitude of the free stream velocity of the heating medium, m/s
$t$	Time, s
$T$	Temperature, °C
$T_i$	Initial product temperature, °C
$T_f$	Film temperature, $1/2(T_o + T_s)$ , °C
$T_o$	Free stream temperature of the heating medium, °C
$T_s$	Product surface temperature, °C
$\alpha$	Thermal diffusivity of the heating medium, $k/(\rho C_f)$ , $\text{m}^2/\text{s}$
$\alpha_p$	Thermal diffusivity of the food product, $k_p/(\rho_p C_p)$ , $\text{m}^2/\text{s}$
$\mu$	Viscosity of the heating medium, kg/ms
$\rho$	Density of the heating medium, $\text{kg/m}^3$
$\rho_p$	Density of the food product, $\text{kg/m}^3$

## INTRODUCTION

The consumer demand for convenient, high quality meals has been growing over the last years. This evolution has stimulated the development of new food processing practices and technologies. The cook-chill method uses mild processing conditions (pasteurisation) to preserve the fresh-like quality of the original ingredients in combination with a cold storage period before consumption or further processing (Light & Walker, 1990). Additionally, in the 'sous vide' method, the thermal processing is performed under vacuum conditions in an air impermeable container to retain better the aroma's and to prevent growth of aerobic micro-organisms and inhibit oxidation reactions (Verboven *et al.*, 1995).

In these methods, several steps during the thermal processing may involve restricted heat transfer: from (re)heating in forced-convection-ovens to chilling in air-blast-chillers and storage in cooling-rooms or display cabinets. A description of these types of equipment and their applications is given by Light & Walker (1990) and Schellekens & Martens (1992). To indicate typical operating conditions, measured air speeds in a forced-convection-oven range from almost 0 m/s up to 6 m/s. Because of the limited heat transfer, hazardous micro-organisms may survive the heat treatment and spoil or contaminate the food during cold storage. Accurate design and control of the heat processing chain is therefore required to reduce the microbial risk to a minimum.

The practical implementation of traditional methods, such as microbial challenge tests (Gorris, 1994), is tedious if they are used to investigate different alternative

processing conditions or if the effect of process deviations is to be established (Nicolai *et al.*, 1996). Alternatively, there is a growing interest in computer simulation tools for the design of thermal food processes, which often involve a combination of heating, cooling and storage (Nicolai *et al.*, 1994). This approach allows a fast and cheap evaluation of the process in terms of safety and quality of the product. Such a tool can as well be used for the evaluation of process deviations and process optimisation as for operator training. These methods use mathematical models for microbial growth and inactivation and degradation of quality (Van Impe *et al.*, 1992) and the heat transfer in the product by which they are affected (Nicolai & De Baerdemaeker, 1996). The actual conditions imposed in the processing equipment are taken into account as boundary conditions at the surface of the food. For conduction heated foods, these consist of the process temperature and the surface heat transfer coefficient (Incropera & De Witt, 1990).

The boundary conditions need to be well known for the heat transfer calculations to be interpreted correctly. The restricted heat transfer in the above mentioned methods is reflected in a small value of the surface heat transfer coefficient, which is often lower than  $30 \text{ W m}^{-2} \text{ K}^{-1}$ . It has been shown that when the surface heat transfer coefficient is small, small deviations in its value may result in large deviations in the food product temperature (Nicolai & De Baerdemaeker, 1996). Furthermore, the value of the surface heat transfer coefficient varies along the surface of the product, as is known from boundary layer theory (Incropera & De Witt, 1990). Taking these facts into consideration, it can be expected that the product temperature distribution is affected by the variation of the local surface heat transfer coefficient along the surface of the food product.

Traditionally, only the product-averaged surface heat transfer coefficients are determined experimentally or derived from existing correlations. An overview of values and mathematical correlations can be found in the literature (Morgan, 1975; Arce & Sweat, 1980; Anon, 1993, 1995; Altomare, 1994). Experimentally determined coefficients and correlations are only applicable for the specific conditions they were derived for, which shows the practical limitation of their use in process evaluation and optimisation studies. Furthermore, the large variation in correlations for average surface heat transfer coefficients discloses the large uncertainty associated with these correlations. Morgan (1975) calculated percent coefficients of variation ranging from 10 to 49% for various correlations for cross flow over circular cylinders. Incropera & De Witt (1990) report comparable accuracy limits.

For the restricted heat transfer conditions under study, taking into account the local character of the surface heat transfer coefficient may improve the accuracy of the calculations of food product temperatures. For simple geometrical shapes (circular, elliptical and rectangular shapes and spheres), the local distribution of the surface heat transfer coefficient has been studied by experimental investigation (Boulos & Pei, 1974; Achenbach, 1975; Kondjoyan & Daudin, 1995; Igarashi, 1985; Igarashi, 1986, 1987; Baughn & Saniei, 1991) and by numerical simulation (Jain & Goel, 1976; Paolino *et al.*, 1986; Karniadakis, 1988; Yang *et al.*, 1991). Little attention has been paid so far to the study of the variation of the surface heat transfer coefficient around the surface for the complex shape of actual food products.

In this paper, the main objective is to develop a validated model-based method for calculating the convective heat transfer from the processing media in industrial appliances to food products and its effect on the product temperature distribution.

The model predictions will be validated against published convective heat transfer results. In a first stage the study will be applied to the heating by cross flow of air over the food. The effect of the main processing parameters, the magnitude of the velocity and the shape of the product, on the heat transfer rate will be investigated. Comparison will be made between the present method and the traditional approach of estimating the surface heat transfer from correlations or existing values. The advantages and limitations of the present model will be established and future directions for research in this field will be indicated.

## METHOD

Forced convection heat transfer results from the existence of a temperature gradient at the interface between a moving fluid and a solid surface, when both are at different temperatures. The temperature gradient is closely related to the formation of a velocity distribution near the surface, since the velocity varies from a zero value (no slip) at the surface to the free stream velocity  $U_\infty$  associated with the free flow. The calculation of the local heat transfer from the local temperature gradient thus also requires the computation of the related flow field boundary layer around the foods. The development of both boundary layers, depends on the flow characteristics (velocity — magnitude and direction — turbulence intensity), the fluid properties (viscosity, density, conductivity, specific heat), the product surface properties (surface roughness) and the product shape and dimensions. Due to the interaction of these parameters, the boundary layers can be very complex resulting in non-constant temperature gradients near the surface.

For a particular shape, the flow characteristics change with the dimensionless Reynolds number  $Re_D = (U_\infty D/\nu)$ , which may be regarded as the ratio of the inertia and the viscous forces. The characteristic length  $D$  is chosen to be the height (thickness) of the food (see Fig. 1). The following short discussion illustrates the

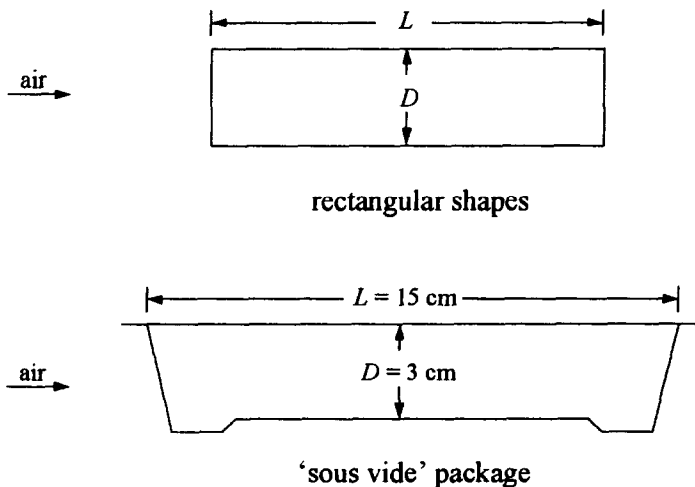


Fig. 1. Food product shapes studied.

Reynolds number dependence of flow past rectangles, if the turbulence in the free stream flow is low. At  $Re_D > 10$ , the inertia forces become considerably larger than the viscous forces, resulting in the flow separating from the leading edges and the formation of vortices downstream of the body. At  $Re_D \approx 100$ , the vortices shed alternately from both sides of the body creating a vortex street which stretches a considerable distance downstream. This zone is also known as the wake. In the case of high width to height ratios  $L/D$  of the rectangle the flow may be complicated by reattachment of the separated flow to the side surfaces. At  $Re_D > 10^3$  turbulent eddies begin to appear in the separated region, contracting the flow due to the action of Reynolds stresses and turbulent entrainment (Okajima, 1982), which ultimately will result in a fully reattached flow and separation from the trailing edges. For a complete description of the influence of the Reynolds number on the flow past smooth rectangles, the reader is referred to Okajima (1982), Davis & Moore (1982) and Igarashi (1987).

In this paper, the two-dimensional food product shapes to be studied are rectangles of different width to height ratios and one actual food product shape (Fig. 1). For the application under study, with air velocities  $U_\infty$  in the range of 0.5 to 6.0 m/s and a product thickness  $D$  ranging from 2 to 10 cm, the range of Reynolds numbers is about  $600 < Re_D < 36,000$ .

### Model equations

It was attempted to model the unsteady, separated and reattached boundary layers with a laminar model, which is solved in a narrow region along the product surfaces. The transport of heat in a system which involves fluid flow can be described by a generic transport equation, when the conservation of energy is applied to an infinitesimal small stationary volume in the flow domain. Because of the low velocity and relatively small pressure gradients, the flow is considered incompressible. For unsteady incompressible flow with no heat production this leads to the following equation:

$$\frac{\partial h}{\partial t} + \nabla \cdot (\mathbf{U}h) - \nabla \cdot (\alpha \nabla h) = 0 \quad (1)$$

Here,  $h$  is the static enthalpy, which is related to the temperature  $T$  through the constitutive equation  $h = h(t, p)$ .  $\mathbf{U} = (u, v)$  is the velocity vector, which contains the 2 air velocity components in the  $x$ - and  $y$ -direction, in a Cartesian reference frame,  $t$  is time and  $\rho$  and  $\alpha$  are the density and the thermal diffusivity of air, respectively. In eqn (1), the work done by the pressure and the viscous forces has been neglected, which is a valid simplification in incompressible flows (Ferziger & Peric, 1996). The velocity field  $\mathbf{U}$  appears in eqn (1), which shows that it must be known in order to solve the equation. The equations describing the air flow can be derived from applying the conservation of mass and momentum, governing the continuity eqn (2) and the momentum eqn (3) (known as the *Navier–Stokes* equations) for incompressible flow:

$$\nabla \cdot \mathbf{U} = 0 \quad (2)$$

$$\frac{\partial \mathbf{U}}{\partial t} + \nabla \cdot (\mathbf{U} \otimes \mathbf{U}) = - \frac{1}{\rho} \nabla p + \nabla \cdot \left( \nu \left( \nabla \mathbf{U} + (\nabla \mathbf{U})^T \right) \right) \quad (3)$$

with  $p$  the pressure and  $\nu$  the kinematic viscosity. In the above equations,  $\nabla \mathbf{V}$  represents the gradient of the vector  $\mathbf{V}$ ,  $\nabla \cdot \mathbf{V}$  is the divergence of the vector  $\mathbf{V}$  and  $\mathbf{A} \otimes \mathbf{B}$  is the tensor product of the matrices  $\mathbf{A}$  and  $\mathbf{B}$ . If the Reynolds number range exceeds the critical value of  $10^3$ , turbulence will be induced in the separated region. Furthermore, flows in industrial food process applications usually are strongly turbulent (Kondjoyan & Daudin, 1995). A few turbulence models (the standard  $k-\varepsilon$  model and the Low Reynolds Number  $k-\varepsilon$  model, Anon, 1995) have therefore been evaluated for their ability to model the complex flow and temperature field. These turbulence models are needed to model additional terms appearing in the flow and energy equations after averaging the equations for the turbulent motions in the flow. They consist of additional semi-empirical transport equations for the variables  $k$  (the turbulent kinetic energy) and  $\alpha$  (the turbulent energy dissipation rate).

To study the effect of the local heat transfer along the surface of the foods on the product temperature, the temperature in the foods must be calculated. Although the model eqns (1–3) can be applied to the whole system of heat transport in the flow, to the product and in the product, which then requires no thermal surface boundary condition, this approach is not feasible from a numerical point of view. Because the vortex shedding is a transient process, which repeats itself at short intervals (for the range of  $D$  and  $U_\infty$  in this application, the period is typically of the order  $10^{-1}$  s), a transient solution procedure with a very small time step is needed to resolve the shedding. With the computational power available it would therefore take too long to solve the model equations for the total required time in a particular thermal process. Alternatively, a separate model is being used for the heat transfer in the product.

Conduction heating foods can be modelled by means of the Fourier equation. This equation can only be solved analytically for simple but unrealistic cases. A finite element numerical solution of the model was accomplished, using the ANSYS version 5.2 finite element program (Swanson Analysis Systems, Houston, USA). Details of the finite element conduction model can be found in Nicolai & De Baerdemacker (1996) and will not be repeated here. The method consists of a geometric representation of the food which is subdivided into a number of elements on which a solution for the Fourier equation is sought. For the rectangular products, 8-node rectangular elements were applied with constant dimensions equal to 1/10 of  $D$ . The 'sous vide' package was covered with a 6-node triangular grid of elements.

### Model parameters

For the rectangles studied, the width to height ratios  $L/D$  were 1, 1.5, 1.7 and 3. The 'sous vide' package of Fig. 1 has approximately a width to height ratio of 5. Because the Reynolds combines the velocity and the characteristic length  $D$  in one parameter, the values for the free stream boundary conditions for velocity were calculated from prescribed values for the Reynolds numbers and  $D$ . The model was used to predict the flow at two low laminar Reynolds numbers,  $Re_D$  equal to 250 and 1000

and three Reynolds numbers in the range of interest, i.e.,  $Re_D$  equal to 5000, 10,000 and 20,000.

The temperature differences were kept small to prevent a large error in the results caused by the temperature dependence of the fluid properties. The inlet temperature  $T_o$  was set to 20°C, the uniform surface temperature  $T_s$  to 40°C. Constant fluid properties for air were chosen at the film temperature,  $T_f$  (Incropera & De Witt, 1990):  $\rho = 1.168 \text{ kg/m}^3$ ,  $\mu = 1.859 \times 10^{-5} \text{ kg/ms}$ ,  $k_f = 0.0265 \text{ W/m}^2 \text{ }^\circ\text{C}$  and  $C_f = 1004 \text{ W/kg }^\circ\text{C}$ . It is noted that the forgoing temperatures do not specifically represent true process conditions, which may lead to small errors when transferring the data to other conditions. A test run was done where the inlet temperature was set at 80°C, which led to a difference of 3% in the calculated product-averaged surface heat transfer coefficient.

The time step was chosen to be 1/80 of an estimated shedding period and a total of about 12 periods were run.

Immobilised water was used as a product. Water properties were determined at a temperature of 52°C, which was chosen to be the average temperature of an initial product temperature of 15°C and a process temperature of 90°C ( $\rho_p = 987 \text{ kg/m}^3$ ,  $C_p = 4182 \text{ J/kg }^\circ\text{C}$  and  $k_p = 0.645 \text{ W/m}^2 \text{ }^\circ\text{C}$ ). The calculated heat transfer coefficients were imposed on the boundary surfaces of the relevant product shape. The use of a local surface heat transfer coefficient was compared to applying a uniform coefficient, equal to the product-averaged surface heat transfer coefficient. The calculations were performed both with the present CFD-calculated surface heat transfer coefficients and the experimental coefficients obtained by Igarashi (1987).

### Computational domain and boundary conditions

The dimensions of the computational domain and conditions imposed are discussed here. Trial and error runs have been conducted to determine the dimensions of the computational domain in order to ensure that the calculation of the flow and temperature field was independent of the location of the boundaries. Sensible dimensions of the computational domain are given in Fig. 2, together with the conditions used on the domain boundaries: uniform parallel flow of air at a pre-set temperature was defined at the upstream and the parallel domain boundaries and zero gradient conditions were imposed normal to the downstream boundary, where the gradient of the normal velocity component needs to be modified to preserve global mass continuity (Versteeg & Malalasekera, 1995). Gradient conditions are known to produce premature smoothing of the flow wake downstream of the product in the calculations (Davis & Moore, 1982), but because of the distance from the boundary to the product it was found not to affect the flow and temperature field in the proximity of the product. At the product surface the normal and tangential velocities were set zero.

A constant surface temperature assumption is made. Traditionally, experimental methods use a constant surface temperature or a constant surface heat flux condition to simplify the analysis (Incropera & De Witt, 1990). Neither of these assumptions correspond to the surface conditions in real food operations, but Kondjoyan & Daudin (1994) report that a constant surface temperature condition is found to be in better agreement with reality than the assumption of a constant surface heat flux condition, relying on an analysis made by Reynolds *et al.* (1960). The former authors estimated the error in the resulting heat flux associated with the

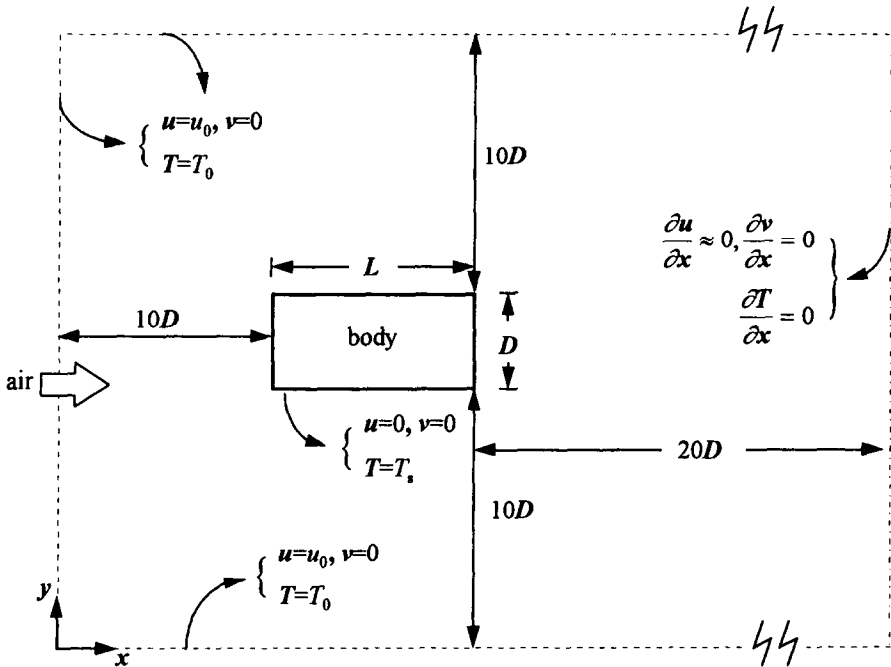


Fig. 2. Definition of the computational configuration.

assumption of a constant surface temperature condition to be 5% for a refrigeration process. The fact that the assumption of constant surface conditions is not completely transferable to industrial conditions is a problem shared by many correlation formulae available.

### Numerical solution method

The second-order partial differential equations cannot be solved analytically. An approximate solution was therefore obtained numerically at discrete points in the computational space around the product.

The numerical solution of the model equations was accomplished by a commercial Computational Fluid Dynamics (CFD) code (CFX 4.1., Harwell, UK), which uses the finite volume method for discretisation (Versteeg & Malalasekera, 1995; Ferziger & Peric, 1996). Relevant aspects of the solution method to the problem under consideration are discussed here, a full description is given in the user manual of the code (Anon, 1995).

The computational domain (Fig. 2) was typically subdivided into 8 blocks on which a grid of control volumes was defined. A non-uniform structured grid was selected with a higher resolution near the product surface. For the laminar and Low Reynolds Number  $k-\epsilon$  model, trial runs with increasingly finer mesh sizes were performed to obtain a solution which was nearly independent on the grid size. The smallest dimension of the cells, near the product surface, was in the range of

$10^{-1}$  mm, the largest dimension of cells, near the domain boundary, was a few cm. The finite volume mesh ranged in size from 7,600 to 13,550 cells, depending on the product shape. Coarser grids were used for the standard  $k-\varepsilon$  model, in which case near-wall profiles were applied.

The model eqns (1–3) are integrated over the control volumes. The resulting space integrals are approximated in terms of the variables located at the fixed control volume centres, i.e., a non-staggered grid is used. The convective terms are discretised using a modified central differencing scheme, called CONDIF, which is second-order accurate. The convection coefficients are calculated from the Rhie–Chow interpolation formula to avoid checkerboard oscillations. Diffusion terms are discretised by second order linear interpolation. The discretisation in time is implicit using the second order Crank–Nicolson method, which is more accurate than backward time stepping for the same grid spacing. Also, the shedding of the flow could not be produced with the backward differencing scheme.

The resulting system of algebraic equations is solved by an iterative solver provided by the code. The variables are taken in sequence and the relevant set of linear equations is solved iteratively for the spatial coupling of the variable, keeping all other variables fixed. The non-linearity and the coupling between the variables are handled by reforming the coefficients of the different terms before each iteration cycle using the most recently updated values of the variables. The SIMPLEC algorithm is used to update the pressure and correct the velocity field so that mass conservation is enforced after each. The convergence error between the iterative solution and the exact solution of the discretised equation was monitored by means of the residuals, which is the amount by which the algebraic discretised equations are not satisfied after an iteration.

A total of 10 iterations per time step was found satisfactory to achieve a low value of all the residuals for all equations. The threshold for the total mass residual was  $10^{-3}$ . At the end of each time step the residuals were typically reduced to less than  $10^{-3}$  of the initial value. Computation times on a HP 9000/720 workstation (64 Mb RAM) were close to 16 h for the finest mesh.

### Calculated characteristics

The following quantities were calculated to characterise the flow, which allowed for a quantitative validation of the flow predictions against the work of these authors. The frequency of shedding is a flow characteristic which value is affected by the Reynolds number of the flow. It is expressed non-dimensionally as the Strouhal number  $S = fD/U$ , with  $f$  the shedding frequency,  $D$  the characteristic length of the body and  $U$  the free stream velocity. The frequency  $f$  was obtained from the Fourier transformation of the predicted time signal of the calculated  $x$ -component of the velocity at a monitor point in the wake behind the product. For this purpose, a short MATLAB-program was written (The MathWorks Inc., Natick, USA). The flow over rectangular bodies is further characterised by a typical drag force, which, for the range of  $Re_D$  studied, are mainly created by pressure drag. This force is characterised by the dimensionless drag coefficient  $C_D$  defined as the ratio of the total drag force per unit area to  $\rho U^2/2$ , which can be easily calculated from the model predictions of the pressure on the surface.

The local surface heat fluxes and the constant surface temperature were stored for each time step. The local fluxes were averaged out over the total time period to

obtain the time-averaged fluxes, from which the time-averaged local surface heat transfer coefficients  $h_x$  were derived. Integration of  $h_x$  over the product surface led to the product-averaged surface heat transfer coefficients  $\bar{h}$ . The coefficients were non-dimensionalised in Nusselt number form, governing a local  $Nu_D = h_x D / k_f$  and a product-averaged  $\overline{Nu}_D = \bar{h} D / k_f$ . Non-dimensionalising the results allowed for generalisation, so that for the Reynolds number and  $L/D$  ratios specified, surface heat transfer coefficients can be calculated for different air velocities  $U_\infty$  and product thickness  $D$  satisfying the non-dimensional  $Re_D$ .

The product temperatures are expressed as  $(T - T_o)/(T_i - T_o)$ , with  $T_i$  the initial product temperature and  $T_o$  the process temperature. The Fourier number  $Fo$  is used as the dimensionless time. Each temperature course corresponds to a particular Reynolds number, which incorporates both the flow conditions and the product dimensions. The temperature courses are to be interpreted for the properties of the fluid (air) and product (immobilised water) under consideration and for each particular product shape.

## RESULTS AND DISCUSSION

### Performance of turbulence models

The turbulence models did not produce a local heat transfer distribution that was comparable with experimental results that were obtained from the literature. While the standard  $k-\varepsilon$  model underpredicted the local heat transfer downstream on the product surfaces parallel to the flow, the Low Reynolds Number  $k-\varepsilon$  model overpredicted these local surface heat transfer coefficients. The product-averaged surface heat transfer coefficients were underpredicted with the standard  $k-\varepsilon$  model and overpredicted with the Low Reynolds Number  $k-\varepsilon$  model.

It is believed by the authors that the assumptions made in the models were not applicable for solving the boundary layer in separated and reattached flows. The relation between the two turbulent variables  $k$  and  $\varepsilon$  in the  $k-\varepsilon$  model is derived for equilibrium flows in which the rates of production and destruction of turbulence are nearly balanced. This assumption has been proven to be valid only in high Reynolds number flows (Versteeg & Malalasekera, 1995) and relatively far from the wall in the so-called log-layer region of the boundary layer. At low Reynolds numbers (smaller than 30,000), as in the present case, and near the wall, the assumption does not hold and an overproduction or -destruction of turbulent kinetic energy is likely to occur when the standard  $k-\varepsilon$  model is used, which is believed to cause the errors in the surface heat transfer calculations. Furthermore, the transition point of the near-wall linear boundary layer and the log-layer depends on the flow type and geometry and has to be incorporated by an empirical parameter in the turbulence model, which is not known exactly in the present case. Near the wall, viscous stresses take over from the turbulent ones and this has to be taken into account by damping the turbulent eddy viscosity and modifying the model equations to incorporate a viscous contribution. This results in the Low Reynolds Number  $k-\varepsilon$  model in which case the model has to be resolved for the viscous sublayer in a narrow region near the wall. Nevertheless, the point at which the viscous stresses start to dominate over the turbulent stresses depends on the flow type and geometry, and can again only be incorporated by additional experimental parameters in the wall

damping functions. In the present study the turbulence models have been used for a fixed set of experimental parameters. Although they have proven to be valid for a wide variety of flows, it is likely they have poor quality for the complex separating and reattaching flow under study. Considerable efforts are currently being invested into the further development of the Low Reynolds Number  $k-\epsilon$  model to deal with separating and reattached flows. The reader is referred to Launder (1988), Abe *et al.* (1994) and Rhee & Sung (1996).

Presently, the laminar model did produce surface heat transfer coefficients that were in best agreement with the experimental data. These results are presented next. The resulting error in the local heat transfer coefficients can be assigned to the inability of the model to capture the small scale turbulent structures in the boundary layer flow. As will be presented, acceptable agreement of the flow characteristics as well as the local heat transfer to experimental data was obtained.

### Flow field predictions

In Fig. 3 a typical flow prediction over a rectangle is given, using a numerical flow visualisation technique (Anon, 1995). The lines in Fig. 3 represent the trajectory of small fluid particles. The model succeeded in predicting the separated flow from the leading edges and the vortex shedding from the trailing edges.

The calculated flow characteristics are given in Table 1 for the cases studied, together with values found in the given references. The two values given for the reference Strouhal number at  $L/D = 1$  and  $Re_D = 1,000, 10,000$  and  $20,000$ , obtained from different publications, indicate the range of variation associated with the Strouhal numbers published for these flows. For the low Reynolds number range a reasonable agreement of the calculations with literature values is found for both the Strouhal number and the drag coefficient. The calculated drag coefficients are lower than the reference values, but they both increase with increasing Reynolds number.

For the high Reynolds number range no drag coefficient was calculated, because no reference values could be found in the literature sources. It is seen that

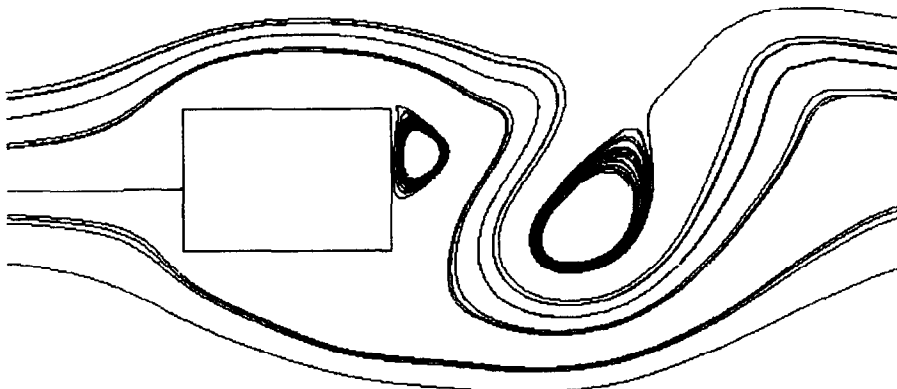


Fig. 3. Flow of a rectangular product;  $L/D = 1.5$ ,  $Re_D = 10,000$ , CFD result.

especially for a  $Re_D$  of 20,000, the calculated Strouhal number differs consistently from the values found in literature for the different  $L/D$  ratios. At  $Re_D = 20,000$  the flow is strongly turbulent which is probably not captured by the presented model. Especially good agreement is found for a  $Re_D$  of 10,000, although the corresponding flow is turbulent in the separated region. The reason for the large difference in Strouhal number for  $L/D = 3$  and  $Re_D = 5,000$  is less clear.

### Surface heat transfer coefficients

Table 2 summarises the product-averaged  $\overline{Nu_D}$  numbers for the high Reynolds number range, which are compared with the results published by Igarashi (1985, 1986, 1987). Figures 4 and 5 show the distribution of the local coefficients  $Nu_D$  for the case of  $L/D = 1.5$  and different Reynolds numbers studied, again together with the experimental pattern obtained from Igarashi (1987).

The general pattern of the predicted local surface heat transfer coefficients agrees with the experimental one. From Fig. 4 it can be seen that on the side surfaces BC and AD, the heat transfer increases from a minimum value at the leading edges, where separation occurs to a high value at the trailing edges. However, important local differences between the calculations and the experiments can be found.

**TABLE 1**  
Strouhal Numbers and Drag Coefficients for Flow over Rectangle Bodies

$L/D$	$Re_D$	$S$		$C_D$	
		Present study	References <sup>a</sup>	Present study <sup>b</sup>	References <sup>a</sup>
<i>1. Low Reynolds number</i>					
1	225	0.16	0.14	1.50	1.77 <sup>c</sup>
	1000	0.13	0.12/0.142	1.98	2.05
1.7	250	0.16	0.170	1.29	1.55
	1000	0.16	0.186	1.67	1.82
<i>2. High Reynolds number</i>					
1	5,000	0.13	0.13		
1	10,000	0.13	0.13/0.14		
	20,000	0.16	0.13/0.14		
1.5	5,000	0.13	–		
	10,000	0.13	0.11		
	20,000	0.16	0.11		
3	5,000	0.19	0.16		
	10,000	0.16	0.11		
	20,000	0.13	0.16		

<sup>a</sup>References: Okajima (1982); Davis & Moore (1982); Igarashi (1987).

<sup>b</sup>Instantaneous values at a particular step.

<sup>c</sup>Time averaged value for  $Re_D = 250$  (Davis & Moore, 1982).

**TABLE 2**  
Product-Averaged Surface Heat Transfer

$L/D$	$Re_D$	$\overline{Nu}_D$		Difference (%) <sup>c</sup>
		CFD present study	Experimental <sup>a</sup>	
1	5,000	37.8	38.7 <sup>b</sup>	2
	10,000	54.0	61.1	12
	20,000	83.1	96.6	14
1.5	5,000	32.6	33.9+	4
	10,000	48.8	53.8	9
	20,000	82.3	85.5	4
3	5,000	27.7	—	
	10,000	41.2	—	
	20,000	68.3	—	
'Sous vide' package	4,545	18.1	—	
	9,090	25.7	—	

<sup>a</sup>Reference: Igarashi (1985, 1986, 1987).

<sup>b</sup>Extrapolated value.

<sup>c</sup>Absolute difference in proportion to the experimental value.

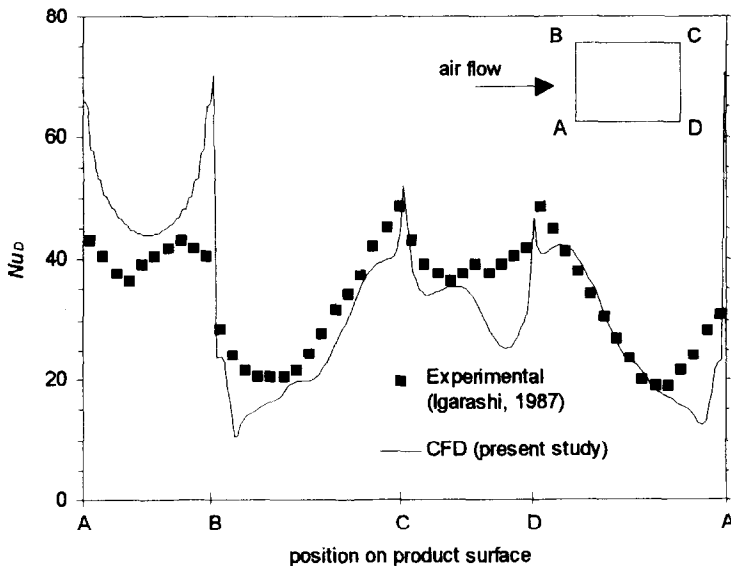


**Fig. 4.** Distribution of the local heat transfer on a rectangular shape;  $L/D = 1.5$ ,  $Re_D = 5,000$ .

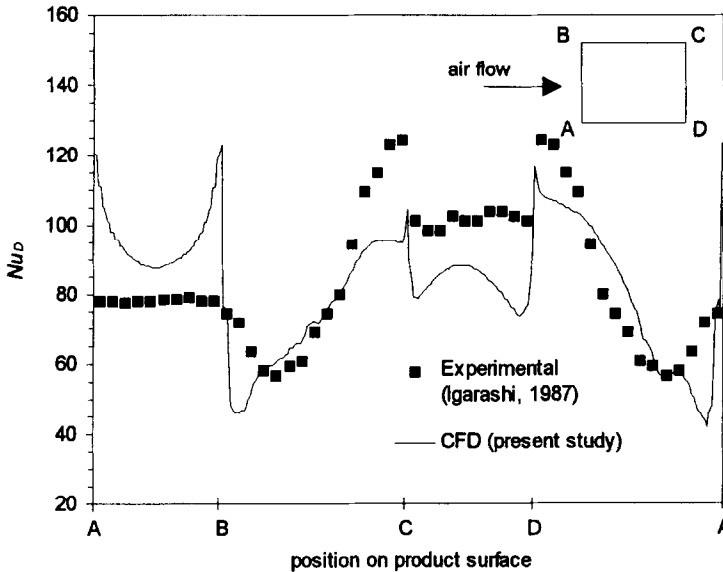


Fig. 5. Distribution of the local heat transfer on a rectangular shape;  $L/D = 1.5$ ,  $Re_D = 20,000$ .

According to the experimental pattern, the heat transfer on the surface AB exposed to the free should have high and nearly constant heat transfer rates. With the model much higher transfer rates are predicted towards the leading edges. A two-fold explanation can be formulated. Firstly, due to the pressure drop downstream towards the leading edges starting from the stagnation point at the middle of the surface AB, the flow is accelerated. This acceleration is probably overpredicted with the laminar model which does not incorporate the damping effect of induced turbulence at this point. Secondly, the finite volume cell in the leading corners has to absorb large fluxes across its boundaries, resulting in a slower convergence of the solution and consequently a lower accuracy than in the rest of the computational domain. Nevertheless, it is believed by the authors that the difference in heat transfer at the corners is not entirely due to an error in the model, supported by the observations of Igarashi (1987) that on the leading surfaces AB the same behaviour as predicted is observed for rectangles with a width to height ratio of 0.33, 1.0 and 1.33, which all had a larger dimension  $D$  than the rectangle with  $L/D = 1.5$ .

The lack of turbulent mixing in the laminar model could explain the relative underprediction on the side surfaces BC and AD directly after separation from the leading edges. The region of reversed flow is more contracted in reality due to the turbulent mixing. It must be noted that experimental values of Igarashi were obtained from a constant surface heat flux condition, while the presented model was used for a constant surface temperature condition. Baughn & Saniei (1991) showed that for the case of circular cylinders, the use of a constant surface temperature condition led to lower Nusselt numbers at the point of separation as compared to a constant flux condition. Kondjoyan & Daudin (1994) also report lower values for the constant surface temperature case, with a mean difference of 10% for a flat plate

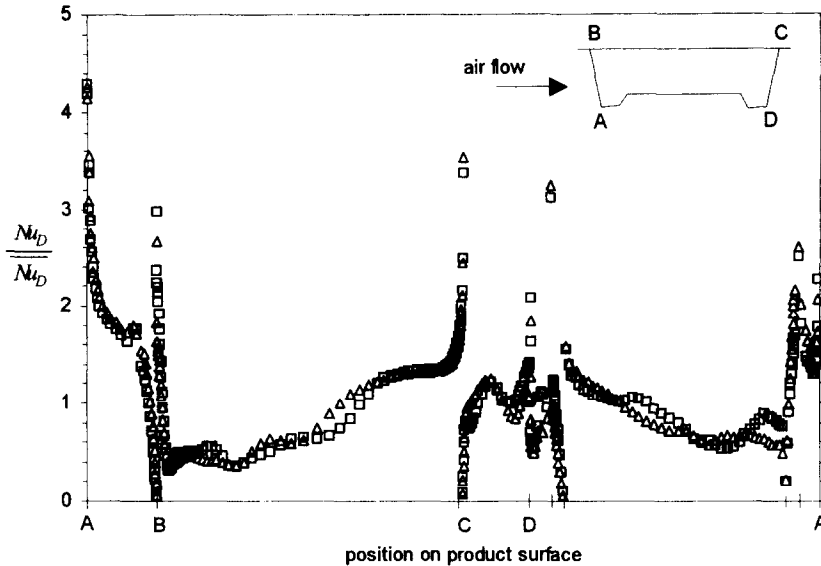


Fig. 6. Normalised distribution of the local heat transfer on a 'Sous vide' package:  $L/D \sim 5$ .  $Re_D = 4,454$  (triangles) and  $Re_D = 9,090$  (squares).

shorter than 1 m and less than 10% for a circular cylinder. Differences of 14% as reported here (Table 2) for the square shapes are probably too large to be caused by the thermal boundary condition alone.

The underprediction of the model on the downstream surface CD can also be attributed to a failure of the laminar model. The lack of turbulent mixing causes an underprediction in the region near the trailing edges where shedding vortices have separated from the surface. Again peaks can be found at the corners, due to the slow convergence of the solution at these points. In general, the combined effect of these features causes the model to consistently underpredict the product-averaged heat transfer rates in all the cases (Table 2), as compared to the experimental data from Igarashi.

The failure of the laminar model is most pronounced in Fig. 5 for the high Reynolds number of 20,000. It is shown that the strong rise in heat transfer rates along the side surfaces BC and AD and on the back surface CD as observed in experiments, caused by an increased turbulent mixing of the separated flow, is not fully captured in the model predictions. Note that the calculated average Nusselt number  $Nu_D$  bar in this case is close to the experimental value (a difference of 4%, Table 2), which illustrates that care must be taken when interpreting the values in Table 2 without looking at the distributions of the local heat transfer rates as presented in the figures.

In Fig. 6 it is shown that for the case of the actual food product shape in the form of the 'sous vide' package, the same pattern of the local surface heat transfer can be recognised, but it is more disturbed, which can be attributed to the reattachment of the flow to the side surfaces in the case of a large  $L/D$  ratio and the more complex

geometry of the 'sous vide' package. The effect of flow acceleration and slow convergence at the edges can again be recognised in the high local heat transfer rates at these points.

### Effect on product temperature distribution

The computed temperature variations are given in Figs 7–9. In Fig. 7, the use of the calculated surface heat transfer coefficient can be compared to applying the coefficients experimentally determined by Igarashi (1987). Because of the underprediction of the calculated surface heat transfer compared to the experimental ones, the centre temperature change in these cases is consistently slower than for the case of using the experimental coefficients.

For the square shape and a rectangle with  $L/D = 1.5$  (Fig. 7), using the local surface heat transfer coefficients or a uniform product-averaged one makes little difference. When the  $L/D$  ratio is increased, the effect of the distribution of the local surface heat transfer coefficients becomes increasingly important. For  $L/D = 3$

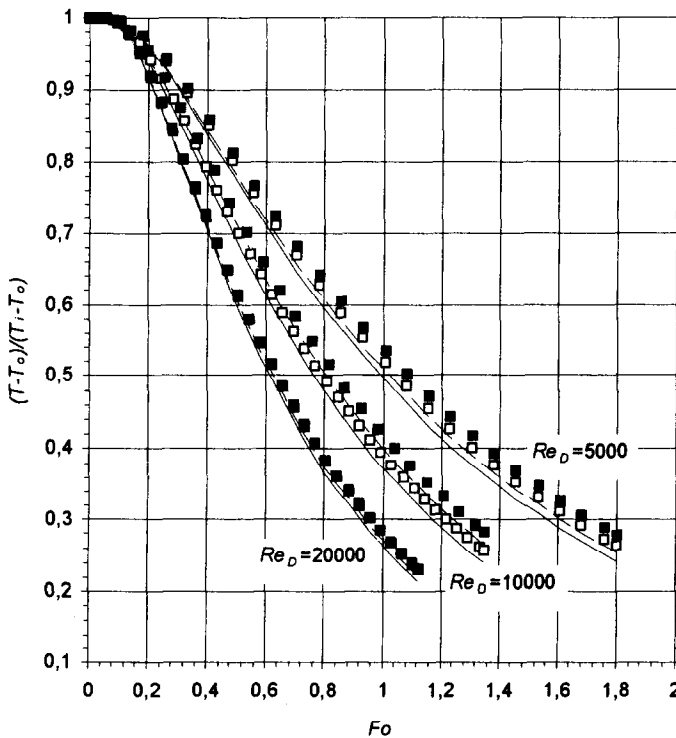


**Fig. 7.** Product centre temperature change for a rectangular shape with  $L/D = 1.5$ . Boundary conditions applied: —, experimental product-averaged surface heat transfer coefficient (Igarashi, 1987); □, experimental local surface heat transfer coefficient (Igarashi, 1987); - -, calculated product-averaged surface heat transfer coefficient (present study); ■, calculated local surface heat transfer coefficient (present study).

(Fig. 8), the effect is most pronounced for the lower Reynolds numbers. Compared to using a uniform surface heat transfer coefficient, the centre temperature change is notably slower when using the local distributions. For  $Re_D = 20,000$ , care should be taken when interpreting the graphs, due to the poor quality of the predictions of the local surface heat transfer coefficients at a Reynolds number of 20,000. For the 'sous vide' package (Fig. 9), the  $L/D$  ratio was approximately equal to 5. The effect of the distribution of the local surface heat transfer coefficient is even more pronounced than for the rectangles with  $L/D = 3$  (Fig. 8), which confirms the increasing importance of the local distribution with increasing  $L/D$ .

The following explanation for the observations can be given. The heat transfer near the centre of slab shaped products (high  $L/D$ ) is mainly one-dimensional, i.e., it is driven by the local conditions on the side surfaces. When the local surface heat transfer coefficient is considerably lower than the uniform one, the product temperature change is expected to be slower. In the case of a low  $L/D$  ratio (Fig. 7), a

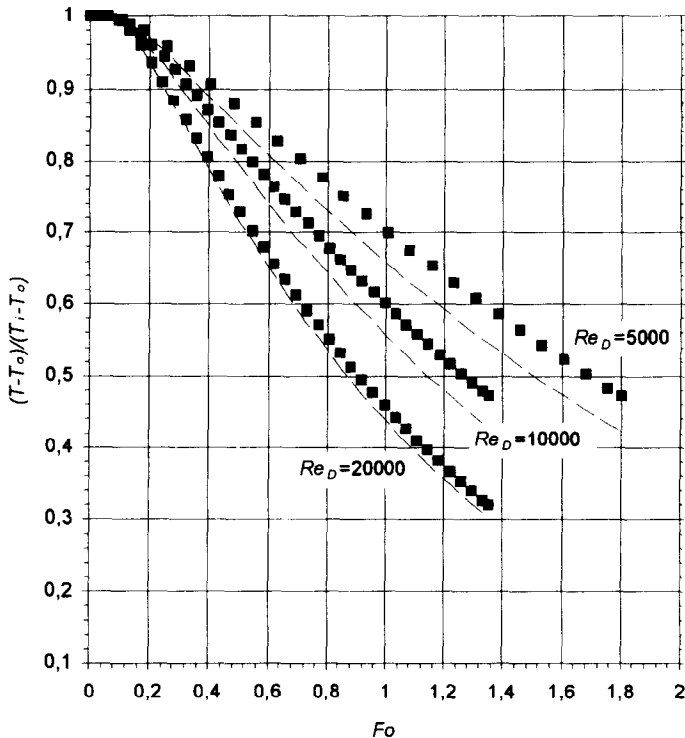


Fig. 8. Product centre temperature for a rectangular shape with  $L/D = 3$  in a cross flow of air. Legend: see Fig. 7, no values for experimental surface heat transfer coefficient available.

**TABLE 3**  
Displacement of the Coldest Spot when Applying Local Surface Heat Transfer Coefficients

$L/D$	$Re_D$	Displacement towards the leading edge	
		General	$D = 3 \text{ cm}$
1	5,000	–	–
	10,000	–	–
	20,000	–	–
1.5	5,000	Less than 1/10 of $D$	–
	10,000		–
	20,000		–
3	5,000	1/4 of $D$	0.75 cm
	10,000	1/3 of $D$	1.0 cm
	20,000	1/10 of $D$	0.3 cm
'Sous vide' package	4,545	6/10 of $D$	1.8 cm
	9,090	6/10 of $D$	1.8 cm

**TABLE 4**  
Product Temperature During Heating with a Cross Flow of Air Products of Different Shapes;  $D = 3 \text{ cm}$ ,  $T_i = 5^\circ\text{C}$ ,  $T_o = 90^\circ\text{C}$

$L/D$	$Re_D$	$t(\text{s})$	$T (^\circ\text{C})$		$\Delta T^b$	
			Local $h^a$	Uniform $h_m$		
			Centre	Coldest spot	Centre	
1	5,000		56.3	–	56.4	–0.1
	10,000	1,300	64.1/65.9	–	64.2/67.0	–0.1
	20,000	1,300	71.7/74.4	–	72.9/75.3	–1.2
1.5	5,000	2,600	66.3/67.6	66.2/67.6	68.8/69.9	–2.6
	10,000	1,950	65.9/68.2	65.9/68.2	67.6/69.9	–1.7
	20,000	1,600	70.4/70.4	70.3/70.2	72.1/71.9	–0.9
3	5,000	2,600	49.6	48.9	54.0	–5.1
	10,000	1,950	49.8	48.6	53.6	–5.0
	20,000	1,650	56.3	56.2	58.0	–1.8
'Sous vide' package	4,545	4,300	51.8	50.1	57.6	–7.5
	9,090	4,300	59.7	57.6	67.0	–9.4

<sup>a</sup>Calculated (present study)/experimental  $h$  (Igarashi, 1987).

<sup>b</sup>Difference between coldest spot (local  $h$ ) and centre (uniform  $h_m$ ).

lower heat transfer rate on the side surfaces can be compensated by the high heat transfer rates on the leading and trailing surfaces (Figs 4 and 5).

Because of the large variation of the local surface heat transfer coefficient on the side surfaces of the shapes, it is further expected that the coldest spot may be moved towards the leading edge of the product, where the local surface heat transfer coefficient on the side surface is the lowest. This is indeed the case, as can be seen in Table 3. For the cases studied, Table 3 summarises the displacements observed in the heat conduction calculations. Although the coldest spot is moved, the temperature difference between the coldest spot and the centre remain small.

To illustrate the findings of this paper in a practical example, in Table 4 calculated product temperatures are listed for a heating process with an initial product temperature of 5°C, a process temperature of 90°C, and for air velocities corresponding to the particular Reynolds numbers. Large errors can occur when neglecting the local character of the surface heat transfer coefficient in the case of slab shaped products and for the cases studied, as indicated in the last column of Table 4. Concerning the displacement of the coldest spot, only for the 'sous vide' package can differences near 2°C be observed between the coldest spot and the centre when using a local surface heat transfer coefficient, which indicates that in this example the displacement of the coldest spot is not severe.

## CONCLUSIONS

The local surface heat transfer could play an important role in many food process. Using a model-based method, a large variation of the local surface heat transfer coefficient around rectangular shaped products was found. During validation, it was found that a laminar model was able to predict the distribution of the surface heat transfer up to Reynolds numbers of 10,000. However, this approach restricts the study to the case of zero turbulence in the free stream. More elaborate modelling is needed to predict heat transfer in turbulent air flows at higher Reynolds numbers. The standard versions of the  $k-\epsilon$  model and its Low Reynolds Number variant were found to be insufficient for this purpose.

It was found that the distribution of the surface heat transfer coefficient is most important for slab-shaped products, in which case the product temperature is driven by the local conditions on the food surface. Using the local instead of the product-averaged surface heat transfer coefficient causes the temperature change in the products to be considerably slower and the coldest spot to be moved slightly towards the leading edge of the heating.

The main conclusion of the presented work therefore concerns the evaluation of the microbial safety of food products. Neglecting the local character of the surface heat transfer coefficients in heat transfer calculations will lead to a higher estimation of the process lethality than is actually the case, caused by an overprediction of the food temperature. Such an improper process design will result in an increased possibility for survival and subsequent growth of hazardous micro-organisms.

## REFERENCES

- Achenbach, E. (1975). Total and local heat transfer from a smooth cylinder in cross-flow at high Reynolds numbers. *International Journal of Heat and Mass Transfer*, **18**, 1387–1396.

- Abe, K., Kondoh, T. & Nagano, Y. (1994). A new turbulence model for predicting fluid flow and heat transfer in separating and reattaching flows — I. Flow field calculations. *International Journal of Heat and Mass Transfer*, **37**, 139–151.
- Altomare, R. E. (1994). Heat transfer in bakery ovens. In *Developments in food engineering*, eds. T. Yano, R. Matsuno & K. Nakamura, Vol. 1, pp. 298–300, Blackie Academic and Professional, London.
- Anon (1993). *American Society of Heating, Refrigeration and Air-Conditioning Engineers handbook — fundamentals*. American Society of Heating, Refrigeration and Air-Conditioning Engineers Inc., pp. 30.20–30.23. Atlanta, USA.
- Anon (1995). *CFX 4.1 Flow solver user guide, CFX 4.1 user manual*. Computational Fluid Dynamics Services, pp. 273–374. Harwell, UK.
- Arce, J. A. & Sweat, V. E. (1980). Survey of published heat transfer coefficients encountered in food processes. *American Society of Heating, Refrigeration and Air-Conditioning Engineers Transactions*, **86**, 2 235–260.
- Baughn, J. W. & Saniei, N. (1991). The effect of the thermal boundary condition on heat transfer from a cylinder in cross flow. *Journal of Heat Transfer, Transactions of the American Society of Mechanical Engineers*, **113**, 1020–1023.
- Boulos, M. I. & Pei, D. C. T. (1974). Dynamics of heat transfer from cylinders in a turbulent air stream. *International Journal of Heat and Mass Transfer*, **17**, 767–783.
- Davis, R. W. & Moore, E. F. (1982). A numerical study of vortex shedding from rectangles. *Journal of Fluid Mechanics*, **116**, 475–506.
- Ferziger, J. H. & Peric (1996). *Computational methods for fluid dynamics*, Vol. 12, pp. 67–78. Springer-Verlag.
- Gorris, L. G. M. (1994). Improvement of the safety and quality of refrigerated ready-to-eat foods using novel mild preservation techniques. In *Minimal processing of foods and processing optimization*, eds. R. P. Singh & F. A. Oliveira, pp. 57–73.
- Igarashi, T. (1985). Heat transfer from a square prism to an air stream. *International Journal of Heat and Mass Transfer*, **28**, 1 175–181.
- Igarashi, T. (1986). Local heat transfer from a square prism to an airstream. *International Journal of Heat and Mass Transfer*, **29**, 5 777–784.
- Igarashi, T. (1987). Fluid flow and heat transfer around rectangular cylinders (the case of a width/height ratio of a section of 0.33 (1.5)). *International Journal of Heat and Mass Transfer*, **30**, 5 893–901.
- Incropera, F. P. & De Witt, D. (1990). *Fundamentals of heat and mass transfer*, 3rd edition, Ch. 2, 6 and 7. John Wiley, New York, Chichester, Brisbane.
- Jain, P. C. & Goel, B. S. (1976). A numerical study of unsteady laminar forced convection from a circular cylinder. *Journal of Heat Transfer, Transactions of the American Society of Mechanical Engineers*, 303–307.
- Karniadakis, G. E. (1988). Numerical solution of forced convection heat transfer from a cylinder in cross flow. *International Journal of Heat and Mass Transfer*, **31**, 1 107–118.
- Kondjoyan, A. & Daudin, J. D. (1994). État des connaissances sur les coefficients de transferts de chaleur et de matière à l'interface air-solide pour un objet isolé lisse. *Entropie*, **186**, 3–16.
- Kondjoyan, A. & Daudin, J. D. (1995). Effects of free stream turbulence intensity on heat and mass transfers at the surface of a circular cylinder and an elliptic cylinder, axis ratio 4. *International Journal of Heat and Mass Transfer*, **38**, 10 1735–1749.
- Launder, B. E. (1988). On the computation of convective heat transfer in complex turbulent flows. *Journal of Heat Transfer, Transactions of the American Society of Mechanical Engineers*, **110**, 1112–1128.
- Light, N. & Walker, A. (1990). *Cook-chill catering, technology and management*, pp. 92–115. Elsevier Applied Science, London, UK.
- Morgan, V. T. (1975). The overall convective heat transfer from smooth circular cylinders. *Advances in Heat Transfer*, **11**, 199–264.

- Nicolăi, B. M., Van Impe, J. F. & Schellekens, M. (1994). Application of expert system technology on the preparation of minimally processed foods: A case study. *Journal A — Special Issue on Advanced Process Control*, **35**, 1 50–55.
- Nicolăi, B. M. & De Baerdemaeker, J. (1996). Sensitivity analysis with respect to the surface heat transfer coefficient as applied to thermal process calculations. *Journal of Food Engineering*, **28**, 21–33.
- Nicolăi, B. M., Verboven, P., Scheerlinck, N., Van Impe, J. F. & De Baerdemaeker, J. (1996). Computer aided food safety design. In *Proceedings of Second European symposium on Sous Vide*, pp. 59–76. Leuven, Belgium.
- Okajima, A. (1982). Strouhal numbers of rectangular cylinders. *Journal of Fluid Mechanics*, **123**, 379–398.
- Paolino, M. A., Kinney, R. B. & Cerutti, E. A. (1986). Numerical analysis of the unsteady flow and heat transfer to a cylinder in crossflow. *Journal of Heat Transfer Transactions of the American Society of Mechanical Engineers*, **108**, 742–748.
- Rhee, G. H. & Sung, H. J. (1996). A nonlinear low-Reynolds-number  $k-\epsilon$  model for turbulent separated and reattaching flows — II. Thermal field computations. *International Journal of Heat and Mass Transfer*, **39**, 16 3465–3474.
- Reynolds, W. C., Kays, W. M. & Kline, S. J. (1960). A summary of experiments on turbulent heat transfer from a non-isothermal flat plate. *Journal of Heat Transfer*, **11**, 341–348.
- Schellekens, M. & Martens, T. (1992). 'Sous Vide' cooking, Part I: Scientific literature review. Study by ALMA University Restaurants, FLAIR, Publication of the Commission of the European Communities, Luxembourg.
- Van Impe, J. F., Nicolăi, B. M., Martens, T., De Baerdemaeker, J. & Vandewalle, J. (1992). Dynamic mathematical model to predict microbial growth and inactivation during food processing. *Applied and Environmental Microbiology*, **58**, 9 2901–2909.
- Verboven, P., Schellekens, M., Nicolăi, B. M., Martens, T. & De Baerdemaeker, J. (1995). The microbiological safety and quality of foods processed by the 'sous vide' system as a method of commercial catering. In *Proceedings of the Food Ingredients Europe '95 Conference*, Frankfurt, Germany.
- Versteeg, H. K. & Malalasekera (1995). *An introduction to computational fluid dynamics. The finite volume method*, pp. 85–133, 196–197. Longman Scientific and Technical, Harlow, England.
- Yang, Y., Chen, C. & Wu, S. (1991). Transient laminar forced convection from a circular cylinder using a body-fitted co-ordinate system. *Journal of Thermophysics*, **6**, 1 184–188.